ELSEVIER

Journal of Volcanology and Geothermal Research 115 (2002) 207–231

Journal of volcanology and geothermal research

www.elsevier.com/locate/jvolgeores

High-resolution aeromagnetic mapping of volcanic terrain, Yellowstone National Park

Carol A. Finn [a,*], Lisa A. Morgan [b]

[a] *U.S. Geological Survey, MS 964, Denver Federal Center, Denver, CO 80225, USA*
[b] *U.S. Geological Survey, MS 966, Denver Federal Center, Denver, CO 80225, USA*

Received 10 April 2001; received in revised form 1 October 2001; accepted 1 October 2001

Abstract

High-resolution aeromagnetic data acquired over Yellowstone National Park (YNP) show contrasting patterns reflecting differences in rock composition, types and degree of alteration, and crustal structures that mirror the variable geology of the Yellowstone Plateau. The older, Eocene, Absaroka Volcanic Supergroup, a series of mostly altered, andesitic volcanic and volcaniclastic rocks partially exposed in mountains on the eastern margin of YNP, produces high-amplitude, positive magnetic anomalies, strongly contrasting with the less magnetic, younger, latest Cenozoic, Yellowstone Plateau Group, primarily a series of fresh and variably altered rhyolitic rocks covering most of YNP.

The Yellowstone caldera is the centerpiece of the Yellowstone Plateau; part of its boundary can be identified on the aeromagnetic map as a series of discontinuous, negative magnetic anomalies that reflect faults or zones along which extensive hydrothermal alteration is localized. The large-volume rhyolitic ignimbrite deposits of the 0.63-Ma Lava Creek Tuff and the 2.1-Ma Huckleberry Ridge Tuff, which are prominent lithologies peripheral to the Yellowstone caldera, produce insignificant magnetic signatures. A zone of moderate amplitude positive anomalies coincides with the mapped extent of several post-caldera rhyolitic lavas. Linear magnetic anomalies reflect the rectilinear fault systems characteristic of resurgent domes in the center of the caldera. Peripheral to the caldera, the high-resolution aeromagnetic map clearly delineates flow unit boundaries of pre- and post-caldera basalt flows, which occur stratigraphically below the post-caldera rhyolitic lavas and are not exposed extensively at the surface.

All of the hot spring and geyser basins, such as Norris, Upper and Lower Geyser Basins, West Thumb, and Gibbon, are associated with negative magnetic anomalies, reflecting hydrothermal alteration that has destroyed the magnetic susceptibility of minerals in the volcanic rocks. Within Yellowstone Lake, which is mostly within the Yellowstone caldera, aeromagnetic lows also are associated with known hydrothermal activity in the lake. Many of the magnetic lows extend beyond the areas of alteration and hot springs, suggesting a more extensive currently active or fossil hydrothermal system than is currently mapped. Steep magnetic gradients, suggesting faults or fractures, bound the magnetic lows. This implies that fractures localize the hot springs.

Magnetic gradient trends reflect the mapped Basin and Range structural trends of north and northwest, as well as northeasterly trends that parallel the regional trend of the Snake River Plain and the track of the Yellowstone hot spot which follow the Precambrian structural grain. These trends are found both at small scales such as in hydrothermal basins and at more regional fault scales, which suggests that the regional stress field and reactivated

* Corresponding author. Tel.: +1-303-236-1345; Fax: +1-303-236-1425.
E-mail address: cfinn@usgs.gov (C.A. Finn).

0377-0273/02/$ – see front matter
PII: S0377-0273(01)00317-1

older structures may exert some control on localization of hydrothermal activity.

Keywords: Yellowstone National Park; aeromagnetic data; geophysical data; geologic mapping; hydrothermal alteration; United States

1. Introduction

Yellowstone National Park (YNP), rimmed by a crescent of older mountainous terrain, has at its core the Quaternary Yellowstone Plateau, an undulating landscape shaped by forces of volcanism and later glaciation. Much of YNP is covered by young sediments, Quaternary volcanic rocks, vegetation, and water, obscuring fracture systems that localized active and fossil hydrothermal systems as well as rhyolitic and basaltic lava flows that formed during early eruptive phases of the Yellowstone caldera. Aeromagnetic data provide a means for seeing through surficial layers and are a powerful tool for delineating crystalline basement beneath cover rocks and estimating depths to the Curie temperature of subsurface rocks in the region (Bhattacharyya and Leu, 1975). However, previously acquired aeromagnetic data were not useful for small-scale geologic mapping. In this paper, we present new low-altitude aeromagnetic data flown with closely spaced flight lines that have been integrated with geologic mapping and magnetic property measurements and compare it with the previously obtained, low-resolution data. Our new data allow us to identify the extent of individual geologic units, fractures, and the distribution of hydrothermally altered areas.

1.1. Geologic framework

YNP is known for its widespread Quaternary volcanic rocks, but much of its northern and eastern portions are covered by Eocene, andesitic volcanic rocks of the Absaroka Volcanic Supergroup (Smedes and Prostka, 1972) and scattered exposures of Paleozoic carbonate rocks and Precambrian granitic gneisses (Fig. 1). These rocks may partially underlie the Quaternary volcanic suite (e.g. Christiansen and Blank, 1972).

Much of the active volcanic and tectonic features are the result of large-scale processes that have been occurring for the past 16 Myr and are now focused at YNP. A series of volcanic fields and nested large calderas has systematically progressed from the 16–14-Ma McDermitt volcanic field on the Oregon–Nevada border northeastward across the Snake River Plain to the Yellowstone Plateau volcanic field (Pierce and Morgan, 1992). Location of the large-scale magmatic and tectonic activity has been controlled by the southwest passage of the North American plate over a thermal plume or disturbance and has been referred to as the track of the Yellowstone hot spot (Zoback and Thompson, 1978; Blackwell, 1989; Leeman, 1982, 1989; Pierce and Morgan, 1992; Smith and Braile, 1994).

Over the past 2 Myr, the Yellowstone volcanic field has evolved through three cycles of caldera-forming activity, each forming its own caldera fracture system and set of pre- and post-caldera lava flows. Within the volcanic field, volcanism of the first cycle at 2.1 Ma was spread over the broad area of the Yellowstone Plateau and produced over 2500 km^3 of pumice and ash culminating with eruption of the Huckleberry Ridge Tuff. This was followed at about 1.3 Ma by eruption of the smaller volume (about 500 km^3) Mesa Falls Tuff, resulting in formation of the Henry's Fork caldera nested in the northwest margin of the first caldera. About 1.23 Ma volcanism shifted back to the northeast for the third and most recent cycle culminating at 0.63 Ma with the eruption of the Lava Creek Tuff from the Yellowstone caldera. All three volcanic cycles in the Yellowstone Plateau followed a similar series of development stages (Christiansen, 1984). Regional tumescence and generation of a ring-fracture system dominated stage 1 (cf. Smith and Bailey, 1968) through which basalt and rhyolite flows erupted intermittently over a relatively long period. Stage 2 was marked by a short climactic episode of cataclys-

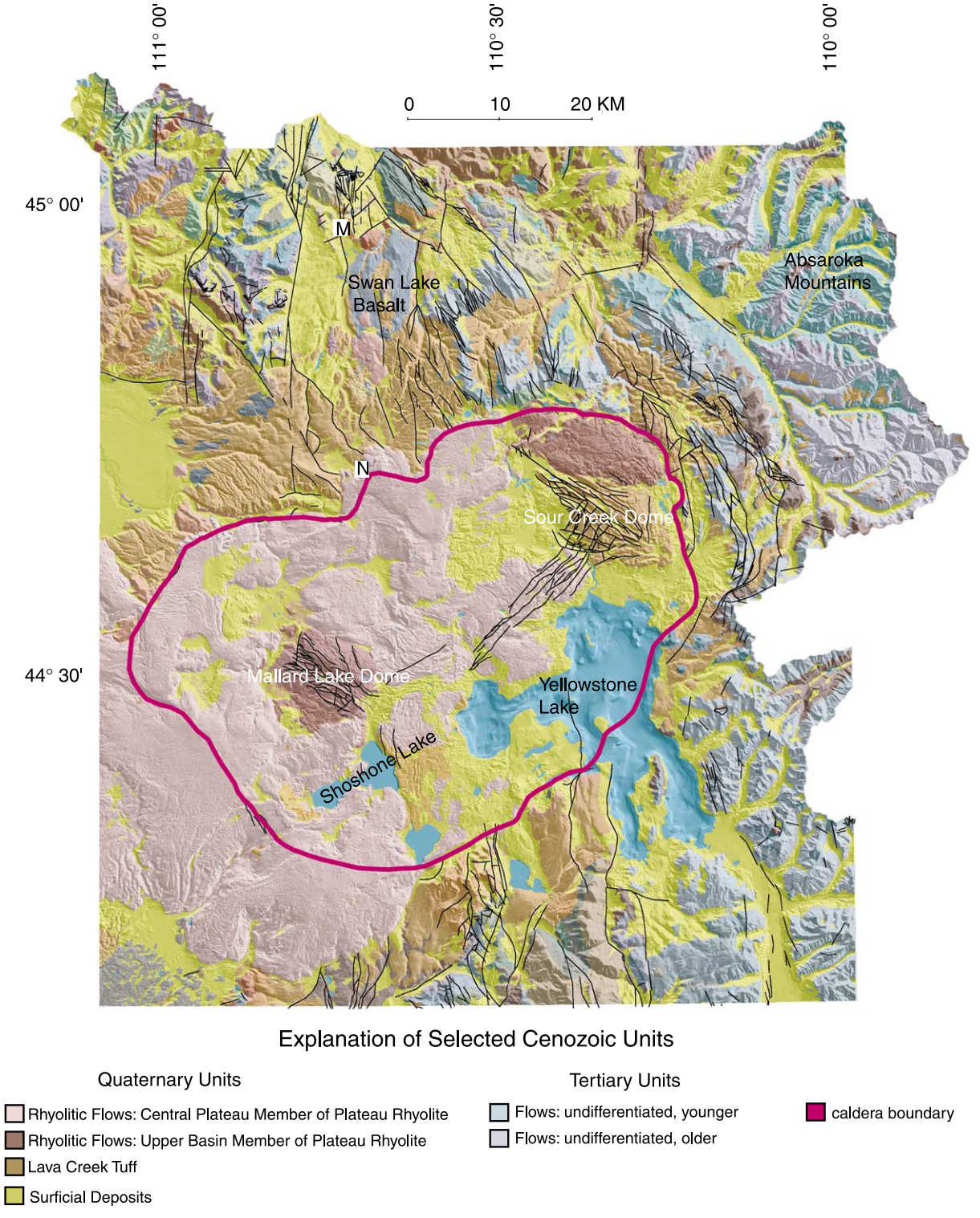
111° 00'
110° 30'
110° 00'
0 10 20 KM
45° 00'
44° 30'
M
N
Swan Lake Basalt
Absaroka Mountains
Sour Creek Dome
Mallard Lake Dome
Yellowstone Lake
Shoshone Lake
Explanation of Selected Cenozoic Units
Quaternary Units
Rhyolitic Flows: Central Plateau Member of Plateau Rhyolite
Rhyolitic Flows: Upper Basin Member of Plateau Rhyolite
Lava Creek Tuff
Surficial Deposits
Tertiary Units
Flows: undifferentiated, younger
Flows: undifferentiated, older
caldera boundary

mic, large-volume, caldera-forming ignimbrite and ash eruptions and was followed by stage 3 where extrusion of rhyolitic lava flows filled much of the caldera and some adjacent terrain. A prolonged period of basaltic volcanism eventually concealed the caldera and comprises stage 4. The latter two stages resulted in the partial to complete filling of the caldera accompanied by solfatara and hot spring activity (cf. Smith and Bailey, 1968). Basalts also erupted intermittently around the margins of the volcanic field during the entire period of rhyolitic activity.

The most recent cycle of volcanism (stage 1) continued for nearly 600 000 yr as rhyolitic lava flows were erupted along the margins of an incipient ring-fracture zone (Fig. 2a). At approximately 0.630 Ma, cataclysmic eruption of more than 1000 km^3 of pumice and ash produced the Lava Creek Tuff (Fig. 2b) removing support from its magma chamber and causing roof collapse along two separate but overlapping ring-fracture systems (Christiansen, 1984). The resulting elongate, northeast-trending Yellowstone caldera is more than 75 km long and about 45 km wide (Fig. 2b). Its boundary is defined by the location of low topography, fault scarps, and rhyolitic lava flow vent locations (Christiansen, 1984). Emplacement of rhyolitic lava flows (Fig. 2c) within the Yellowstone caldera began immediately after eruption of the Lava Creek Tuff. The Sour Creek resurgent dome (Figs. 1 and 2c) was emplaced at about 0.481 ± 0.008 Ma (Gansecki et al., 1996, 1998). Rhyolites erupted in the Mallard Lake resurgent dome (Figs. 1 and 2c) between 0.516 ± 0.007 Ma and 0.198 ± 0.008 Ma (Gansecki et al., 1996, 1998) and at 0.151 ± 0.005 Ma (Christiansen, 1984; Obradovich, 1992). Stage 3 rhyolitic activity continued filling in the Yellowstone caldera during three major pulses at about 0.158 Ma, 0.111 Ma, and 0.070 Ma (Christiansen and Blank, 1972; Christiansen, 1984; Hildreth et al., 1984; Obradovich, 1992) (Fig. 2c). The margins of the caldera have generally been buried by stage 3 volcanism. Basaltic activity, which usually marks the final stage of each caldera cycle, has not yet penetrated the floor of the Yellowstone caldera; however, hydrothermal activity (stages 3 and 4), for which YNP is famous, is widespread (Fig. 2d).

The renowned geysers, hot springs, and fumaroles of YNP may date from renewed magmatic activity that started about 0.158 Ma (Fournier et al., 1976). Several lines of evidence suggest that the magmatic system that is the source of the lavas and heat for the hydrothermal systems is still active with temperatures in excess of 350°C at very shallow depths (Fournier, 1989). Various geophysical anomalies indicate a partially molten magma body underlies large parts of the Yellowstone Plateau (Eaton et al., 1975). In addition, gravity and seismic data have delineated thick sections of fractured, fluid-saturated and altered rock at depths as shallow as 2 km beneath the northeastern edge of the caldera (Lehman et al., 1982). A similar zone of fractured, altered rock has been inferred from electromagnetic (Stanley et al., 1991), seismic, and gravity data (Lehman et al., 1982) along the Norris–Mammoth corridor, north of the north–central caldera boundary. Episodic uplift and subsidence of the caldera floor have been documented in leveling, trilateration (Dzurisin et al., 1990; Pelton and Smith, 1982), GPS, and radar interferometry studies (Wicks et al., 1998). These deformation data are consistent with magmatic fluid migration beneath the caldera.

A belt of active faults (Pierce and Morgan, 1992) and seismicity (Anders et al., 1989; Smith and Braile, 1994) forms a crescent-shaped parabola with its apex at the northeastern end of the Yellowstone Plateau that opens toward the topographically lower eastern Snake River Plain to the southwest, marking the path of the proposed thermal plume. North and west of the caldera and

Fig. 1. Color shaded-relief image of geologic map (colors) (U.S. Geological Survey, 1972) overlain on USGS digital elevation model and bathymetry (Kaplinski, 1991) (shading) of YNP. The magenta line marks the Yellowstone caldera boundary as proposed by Christiansen (in press); the southeast corner of the caldera is modified based on the new high-resolution magnetic data presented in this paper and new bathymetric and seismic data from Yellowstone Lake (Morgan et al., in press). M = Mammoth Hot Springs; N = Norris Geyser Basin.

extending beyond the Park boundary, faults have north, east, and northeast trends, whereas 100 km northwest of the boundary, northwest trends predominate (Pierce and Morgan, 1992). In YNP, the faults generally terminate at the Yellowstone caldera (Locke et al., 1992). The north-trending faults south of the Yellowstone caldera (Fig. 1) define a block-faulted terrain tectonically equivalent to the eastern marginal zone of the Great Basin system of regional tectonic extension (Christiansen and McKee, 1978; Smith and Sbar, 1974). Within the caldera, the major faults trend northeast (Fig. 1). These intersecting fault trends suggest a locus of complex extension in the Yellowstone region.

On a smaller scale, fractures may have influenced the location of specific eruptive vents, much as they appear to control the location of hydrothermal features today (Kaplinski, 1991; Morgan et al., 1977; Muffler et al., 1971). A key to understanding the dynamics of caldera formation and the hydrothermal systems that characterize YNP is the distribution and activity of fracture systems. However, it is often difficult to associate earthquakes in the region with specific faults (Smith and Braile, 1994).

2. Comparison of low- and high-resolution aeromagnetic data

2.1. Low-resolution data

Previous workers at YNP (Bhattacharyya and Leu, 1975; Eaton et al., 1975; Smith et al., 1974) analyzed aeromagnetic surveys flown at relatively constant elevations ranging from 3600 to 4300 m above sea level along east-trending lines spaced 1600 m apart (U.S. Geological Survey, 1973). Magnetic values were collected every 50–75 m along the flight lines. The smallest three-dimensional features that these data can resolve are 1600 m across. Interpretations were based on contour maps of the data (Fig. 3).

The broad magnetic low over the caldera was inferred to reflect shallow, hot silicic upper crust and altered near-surface rocks (Eaton et al., 1975; Smith et al., 1974). From these data, investigators determined a 5- (Bhattacharyya and Leu, 1975) to 10-km (Smith et al., 1974) depth to the bottom of the magnetized crust, assuming a Curie temperature of approximately 580°C. The sources of other local magnetic lows on the map are sedimentary rocks and hydrothermally altered volcanic units (Fig. 3; Eaton et al., 1975).

Magnetic highs in the northern and eastern parts of YNP (Fig. 3) were related to Tertiary volcanic rocks present in the topographically high Absaroka Mountains (Fig. 1). In the southwestern part of YNP, the sources of the highs along the caldera boundary were interpreted as buried terrain composed either of highly magnetized Tertiary andesitic rocks (Eaton et al., 1975) or intrusions (Smith et al., 1974).

Major faults in volcanic rocks appear as linear alignments of closely spaced contours (Fig. 3). The linear northwest-trending gradient along the eastern portion of YNP beyond the northeastern caldera boundary (Fig. 3) was inferred to be a major crustal boundary (Smith et al., 1974). Northwest-trending linear anomalies parallel the Basin and Range structural trends whereas northeast-trending anomalies mimic the structural grain of the regional Precambrian rocks (Eaton et al., 1975). Individual geologic units and local faults, many having smaller dimensions than 1600 m, are difficult to recognize in these low-resolution data.

2.2. High-resolution data

Recent improvements in navigation, data acquisition, processing and imaging capabilities greatly enhance the resolution of modern aeromagnetic data and make it a useful tool for local geologic mapping. The use of real-time differential GPS navigation has decreased location-related errors to less than 2 nT (Grauch and Millegan, 1998). Modern magnetometers have a resolution of 0.01 nT and can cycle every 0.1 s which corresponds to approximately one sample every 5–7 m at typical fixed-wing flight speeds (Denham, 1997). New survey designs with relatively close line spacing (<500 m) and low flight elevations (<350 m draped above the terrain) permit resolution of low-amplitude, short-wavelength magnetic anomalies (Grauch and Millegan, 1998).

New aeromagnetic data over YNP were acquired at an altitude of 350 m above the terrain along north–south-trending flight lines spaced 400 m apart (U.S. Geological Survey, 2000). The aim of this survey was to resolve features at scales useful for mapping individual geologic units, faults, and areas of alteration. To facilitate geologic interpretation, several techniques can be applied to the magnetic data. The first step is to reduce the observed magnetic data to the pole, a technique designed to account for the inclination of the Earth's magnetic field (Fig. 4). Its principal effect is to shift magnetic anomalies to positions directly above their sources (Baranov and Naudy, 1964). An assumption in this correction is that the remanent and induced directions are similar (within about 25°, Bath, 1968). This assumption holds for much of the area (see Table 1).

To differentiate topographic from geologic effects, we calculate a magnetic map associated with terrain and compare it qualitatively with the observed data. Several assumptions are made in the calculation. We assume that the terrain is uniformly magnetized in the present Earth's field direction (inclination of 70°, declination of 15°) and has a magnetic intensity of 2.5 A/m, similar to values measured for the Quaternary flows and the Lava Creek Tuff (Reynolds, 1977; L.A. Morgan and S.S. Harlan, unpublished data; Table 1). The magnetic anomaly is then calculated from a digital terrain model on the same flight surface as the observed magnetic data and reduced to the pole. Comparison of the observed reduced-to-the-pole magnetic anomalies (Fig. 4) with those caused by uniformly magnetized terrain (Fig. 5) draws attention to areas with buried magnetic sources or places where the surficial lava flows are not as magnetic or are thinner than expected. If the shape of the observed magnetic anomaly mimics that caused by terrain, but the amplitudes of the anomalies are different, this may imply that the topography does contribute to the observed anomaly but has a magnetization different than assumed.

Another way to facilitate geologic interpretation of the magnetic data is to estimate depths to tops of magnetic sources. In order to estimate minimum depths to sources from aeromagnetic data, the magnetic contacts must be located. This is done by applying a function to the aeromagnetic data, called the maximum horizontal gradient that is peaked over the contacts (Blakely and Simpson, 1986; Cordell and Grauch, 1982, 1985). Once crests and strike directions of the horizontal gradient are located, the minimum depth of the contact can be estimated by performing a least squares fit to the theoretical shape of the horizontal gradient over a contact (Phillips, 1997, 1999). It is also possible to transform the magnetic data into the magnetic potential (or pseudo-gravity anomalies) in order to simplify the interpretation of magnetic anomalies. Gravity anomalies over tabular bodies have their steepest horizontal gradients over the edges of the bodies, a property that can be exploited in magnetic interpretation by transforming the magnetic data to pseudo-gravity and calculating the maximum of the horizontal gradient to locate edges (Blakely, 1995). In this case, estimates from the horizontal gradient of the pseudo-gravity field represent maximum depths (Phillips, 1999). Comparison of the depths derived from the reduced-to-the-pole (Fig. 6a) and pseudo-gravity (Fig. 6b) data shows that the minimum depth to the tops of most sources within the caldera and along the Norris–Mammoth corridor (between N and M, Fig. 4) is at the surface (Fig. 6a) while the maxima are generally above about 600 m (Fig. 6b). This indicates that observed magnetic anomalies likely reflect the near-surface geology. If the minimum depths exceed the average thickness of surface units (about 1000 m) (Fig. 6a), the source of observed magnetic anomalies may not be related to geologic units near the surface.

Faults and fractures commonly produce linear crests in the horizontal gradients of the aeromagnetic data. To highlight trends in the aeromagnetic data, we digitized linear patterns of the peaks in the magnitude of the horizontal gradient of the reduced-to-the-pole and pseudo-gravity transformations of the aeromagnetic data that we used for the depth calculations (Fig. 6). The lineaments delineated from the pseudo-gravity gradients represent deeper or more regional boundaries than those drawn from the reduced-to-the-pole gradients (Fig. 7).

Table 1
Susceptibility, NRM and total magnetization vectors for selected units at YNP

Geologic name	Lat.	Long.	NRM vector			Volume susceptibility average	Q	Total magnetization vector		
	(°N)	(°W)	Dec. (°)	Inc. (°)	A/m average	SI units		Dec. (°)	Inc. (°)	A/m average
Members of the Plateau rhyolite post-caldera rhyolites										
intra-caldera										
Solfatara Plateau flow	44.7259	110.5394	4.5	64.2	4.57E+00	6.46E−04	2.26E+01	5.1	64.7	4.94E+00
Dry Creek flow	44.4429	110.6893	325.9	62.9	5.56E+00	5.04E−04	2.22E+01	327.5	63.6	5.83E+00
Upper Basin member*	44.4427	110.8102	4	55.6	2.90E+00	6.38E−04	9.09E+00	4.7	57.3	3.25E+00
Upper Basin member*	44.7499	111.5024	346.7	62.8	5.26E+00	4.27E−04	2.38E+01	347.6	63.2	5.50E+00
extra-caldera										
Obsidian Creek member*	44.8862	110.742	358.2	60.9	2.90E+00	5.83E−04	9.86E+00	359.4	62	3.23E+00
post-caldera basalts										
Madison River basalt	44.6608	111.0558	336.8	65.7	6.72E+00	9.09E−04	1.77E+01	338.9	66.3	7.22E+00
Swan Lake Flat basalt	44.9109	110.7421	346.1	58.7	1.16E+01	1.45E−03	1.65E+01	347.3	59.6	1.24E+01
Yellowstone Group										
Lava Creek Tuff	44.1314	111.6672	4.9	64.6	5.94E+00	6.02E−04	2.13E+01	5.3	65	6.28E+00
Pre-caldera rhyolite										
Lewis Canyon rhyolite	44.1519	110.6778	357.5	48.5	6.97E−01	2.14E−04	6.68E−01	358.9	51.9	8.10E−01
Lewis Canyon rhyolite	44.1931	110.6596	151.3	−50.5	5.18E−01	6.95E−04	1.53E+00	130.6	−5.7	2.54E−01
Absaroka Volcanic Supergroup										
Lake Butte intrusion	44.5181	110.2849	170	−40.8	1.76E−01	1.18E−03	3.01E−01	44.8	77.7	5.33E−01
Lake Butte intrusion	44.5136	110.2717	171.2	−39.8	2.28E+00	2.02E−03	2.36E+00	165.1	−14.7	1.46E+00
Langford Formation	44.4918	110.033	349.3	69.1	1.52E+00	1.89E−03	1.60E+00	359.3	70.3	2.59E+00
Absaroka Volcanic	44.4952	110.208	168	−53.4	1.69E+00	4.48E−03	7.79E−01	113.3	66.4	1.15E+00
Supergroup dike										

Earth's field inclination = 70°, declination = 15 ° and an intensity of 56 100 nT was used in the calculation of the total magnetization vector; Q = Koenigsberger ratio.

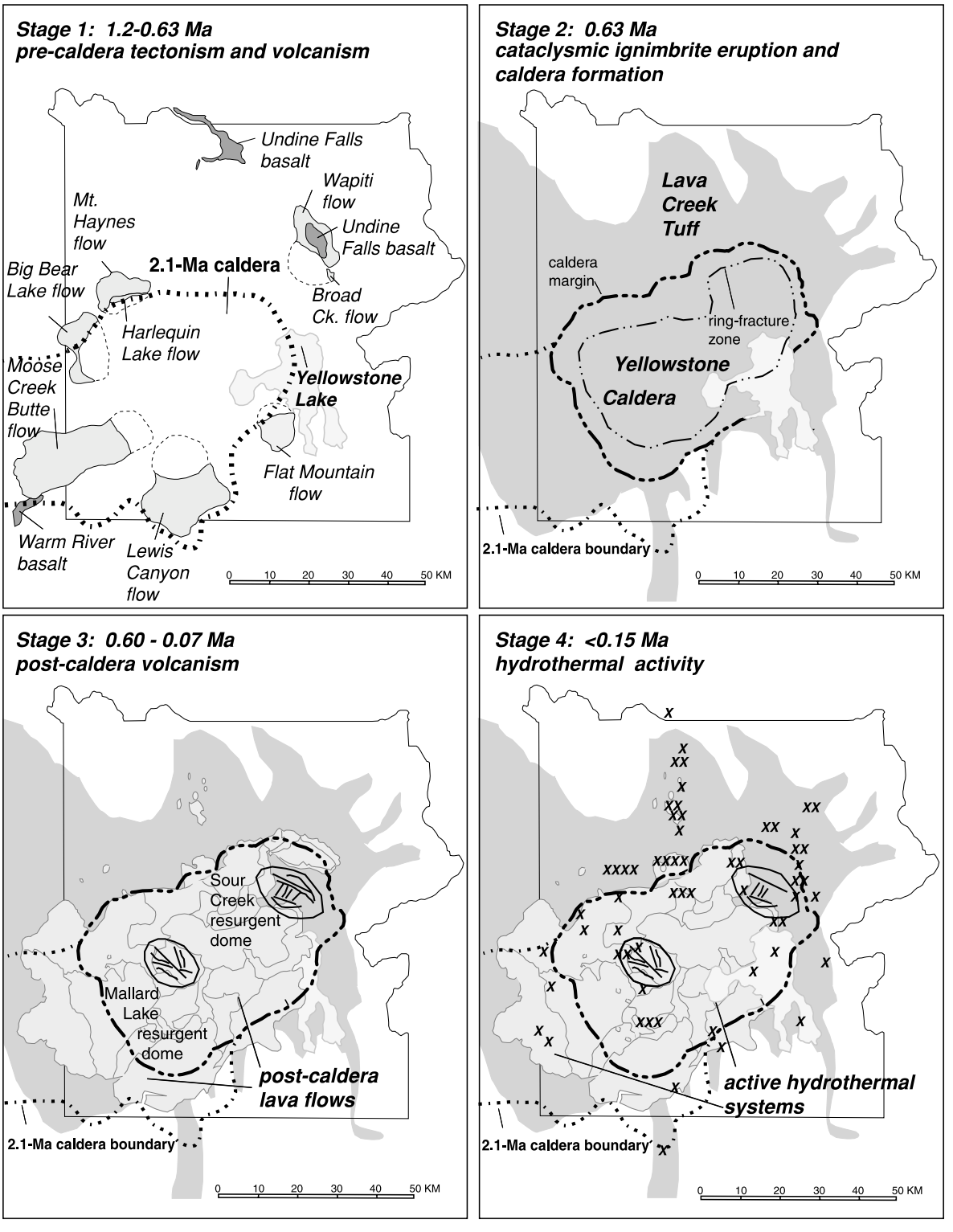
Stage 1: 1.2-0.63 Ma
pre-caldera tectonism and volcanism
Undine Falls basalt
Wapiti flow
Mt. Haynes flow
Undine Falls basalt
Big Bear Lake flow
2.1-Ma caldera
Broad Ck. flow
Harlequin Lake flow
Moose Creek Butte flow
Yellowstone Lake
Flat Mountain flow
Warm River basalt
Lewis Canyon flow
0 10 20 30 40 50 KM
Stage 2: 0.63 Ma
cataclysmic ignimbrite eruption and
caldera formation
Lava Creek Tuff
caldera margin
ring-fracture zone
Yellowstone Caldera
2.1-Ma caldera boundary
0 10 20 30 40 50 KM
Stage 3: 0.60 - 0.07 Ma
post-caldera volcanism
Sour Creek resurgent dome
Mallard Lake resurgent dome
post-caldera lava flows
2.1-Ma caldera boundary
0 10 20 30 40 50 KM
Stage 4: <0.15 Ma
hydrothermal activity
active hydrothermal systems
2.1-Ma caldera boundary
0 10 20 30 40 50 KM

3. Utility of aeromagnetic data for mapping geology and alteration

Interpretation of aeromagnetic data in Yellowstone is difficult for several reasons. Remanent magnetization intensities and magnetic susceptibilities vary widely, sometimes within the same unit (Table 1; Reynolds, 1977; Oliver and Christiansen, 1998; L.A. Morgan and S.S. Harlan, unpublished data). The vector sum of the remanent and induced components of the magnetic field, the total magnetization, is reflected in the patterns on the aeromagnetic map. In this volcanic region, magnetic lows can be caused by, (1) topographically low areas, (2) hydrothermally altered volcanic rocks, (3) reversely magnetized igneous rocks, or (4) non-magnetic rocks. Normally magnetized, fresh volcanic rocks in topographically high areas commonly cause magnetic highs. The presence of rugged topography composed of strongly magnetic rocks complicates the interpretation of aeromagnetic data (Grauch and Hudson, 1987; Grauch et al., 1997). Positive correlation of anomalies with topography suggests that rocks that compose the elevated terrain are normally magnetized. An inverse correlation can be inferred for reversely magnetized rocks in areas of high terrain (Grauch et al., 1997). Lack of correlation with topography or with the mapped extent of geologic units suggests that the magnetic sources underlie units exposed at the surface. Understanding the relation of magnetic anomalies to surficial and buried rocks in YNP is best accomplished by comparing observed magnetic anomalies with those expected from the topography, extent of mapped units, and using input from rock-magnetic property measurements (Grauch et al., 1997).

Detailed rock-magnetic studies for several volcanic units were conducted (Table 1). The volume susceptibility and natural remanent magnetization (NRM) values were averaged for each unit (L.A. Morgan and S.S. Harlan, unpublished data). Total magnetizations were calculated by adding the NRM values and induced component, which was obtained by multiplying the magnetic susceptibility by the intensity of the present Earth's field at the study area (56 100 nT). Susceptibilities range from about 2×10^{-4} to 5×10^{-3} SI. NRM intensities range from 0.6 to 7 A/m. Most of the measured NRM polarities are normal; reversed polarities are concentrated in the Tertiary igneous suites with the exception of the Quaternary pre-caldera Lewis Canyon and Harlequin Lake rhyolite flows.

The total magnetization intensities for the Quaternary rocks range from 0.8 to 7.0 A/m with most values above 2.0 A/m. For most of the measured samples, the remanent component dominates the total magnetizations ($Q \gg 1$). The range of total magnetizations (Table 1), along with those measured in other studies (discussed below), indicates that most of the lava flows and intrusions are magnetic enough to produce observable magnetic anomalies.

3.1. Mapping of Tertiary andesitic rocks

The 53.0- to 43.7-Ma volcanic rocks of the Absaroka Province display both normal and reversed magnetic polarities (Harlan et al., 1996; L.A. Morgan and S.S. Harlan, unpublished data; Nyblade et al., 1987; Sundell et al., 1984; Shive and Pruss, 1977; Pruss, 1975). Limited magnetic susceptibility measurements of the Tertiary Absaroka Supergroup range from $6–8\times10^{-3}$ SI in andesitic mudflows to $20–40\times10^{-3}$ SI for a diorite dike, andesitic lava flows, and flow breccias (Table 1; Oliver and Christiansen, 1998). Limited measurements of remanent magnetizations in the Tertiary volcanic rocks range from about 0.2 to 2.0 A/m with a reversed polarity direction in the Lake

Fig. 2. Major late Cenozoic volcanic features of the Yellowstone Plateau volcanic field (compiled and modified after Christiansen, 1984; Christiansen, in press; and Hildreth et al., 1984). (a) Stage 1: dark gray = basalt, light gray = rhyolite. The 2.1-Ma caldera erupted the voluminous Huckleberry Ridge Tuff, (b) stage 2. Shaded area represents a schematic distribution of the caldera-forming Lava Creek Tuff. (c) Stage 3. Dark gray = Lava Creek Tuff, light gray = post-caldera rhyolites. (d) Stage 4. Small x's = locations of hydrothermal activity. The location of Yellowstone Lake is for reference only.

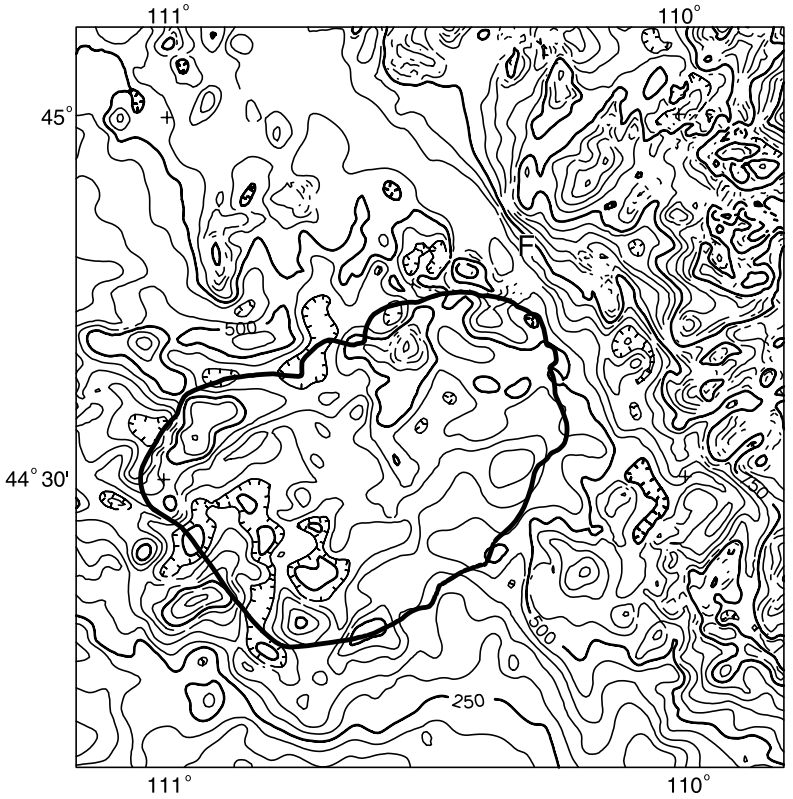

Fig. 3. Magnetic map derived from several old aeromagnetic surveys (U.S. Geological Survey, 1973). Contour interval is 50 nT. Lows are hachured. The bold line marks the Yellowstone caldera boundary.

Butte intrusion and an Absaroka dike (Table 1) (L.A. Morgan and S.S. Harlan, unpublished data). The observed magnetic data (Fig. 4) display only a general correlation with that caused by topography (Fig. 5). Topographic anomalies produced by formations with total magnetization vectors within 25° of the present Earth's field vector (Bath, 1968) and intensities greater than about 2.0 A/m, such as the Langford Formation (Table 1) in the Absaroka Mountains, correlate with the observed aeromagnetic data. Estimates of depths to magnetic sources are greatest beneath the Tertiary rocks (Fig. 6) suggesting that many of the sources are buried, despite the high bulk susceptibility measured at the surface. The amplitudes of the magnetic anomalies in the Absaroka Range (Fig. 1) are higher than those for Tertiary rocks in the western part of YNP and higher than what would be expected from the topography. Eaton et al. (1975) attributed this to volcanic source vents in the east as opposed to alluvial facies in the west.

One of the few places over which the observed magnetic anomaly is positive and the magnetic terrain anomaly negative contains the boundaries of three post-caldera Quaternary rhyolitic flows (locality T, southern part of the Yellowstone caldera, Figs. 4 and 5). Estimates to the depth of the source of this positive anomaly (T, Fig. 6) suggest that it is buried several hundred meters below the surface and therefore is probably not due to the mapped Quaternary lava flows but may instead relate to buried Tertiary andesitic lavas.

The deep, fault-bounded, glacially incised valley beneath the Southeast Arm of Yellowstone Lake (SE, Figs. 4 and 5) produces a linear magnetic low adjacent to magnetic highs. To the east, the magnetic highs are related to the Tertiary andesitic volcanic rocks, as is the magnetic high over the promontory separating the Southeast Arm from

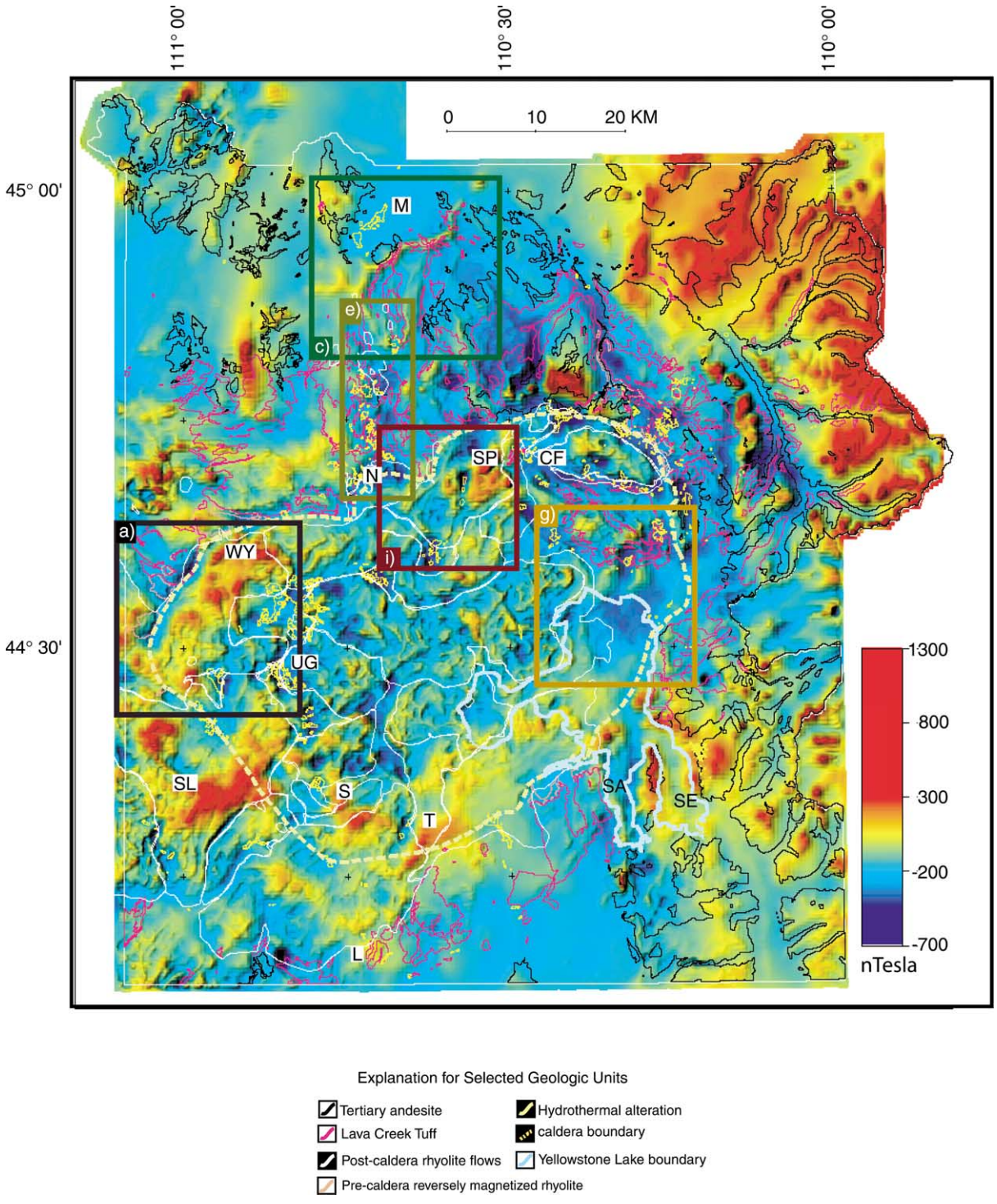

Fig. 4. Color shaded-relief image of high-resolution, reduced-to-the-pole aeromagnetic data. Polygons outline selected geologic units (above) (U.S. Geological Survey, 1972). Outlines of Quaternary lava flows (in white) digitized from Hildreth et al. (1984). Letters denote locations discussed in the text. Boxes outline maps shown in Fig. 8.

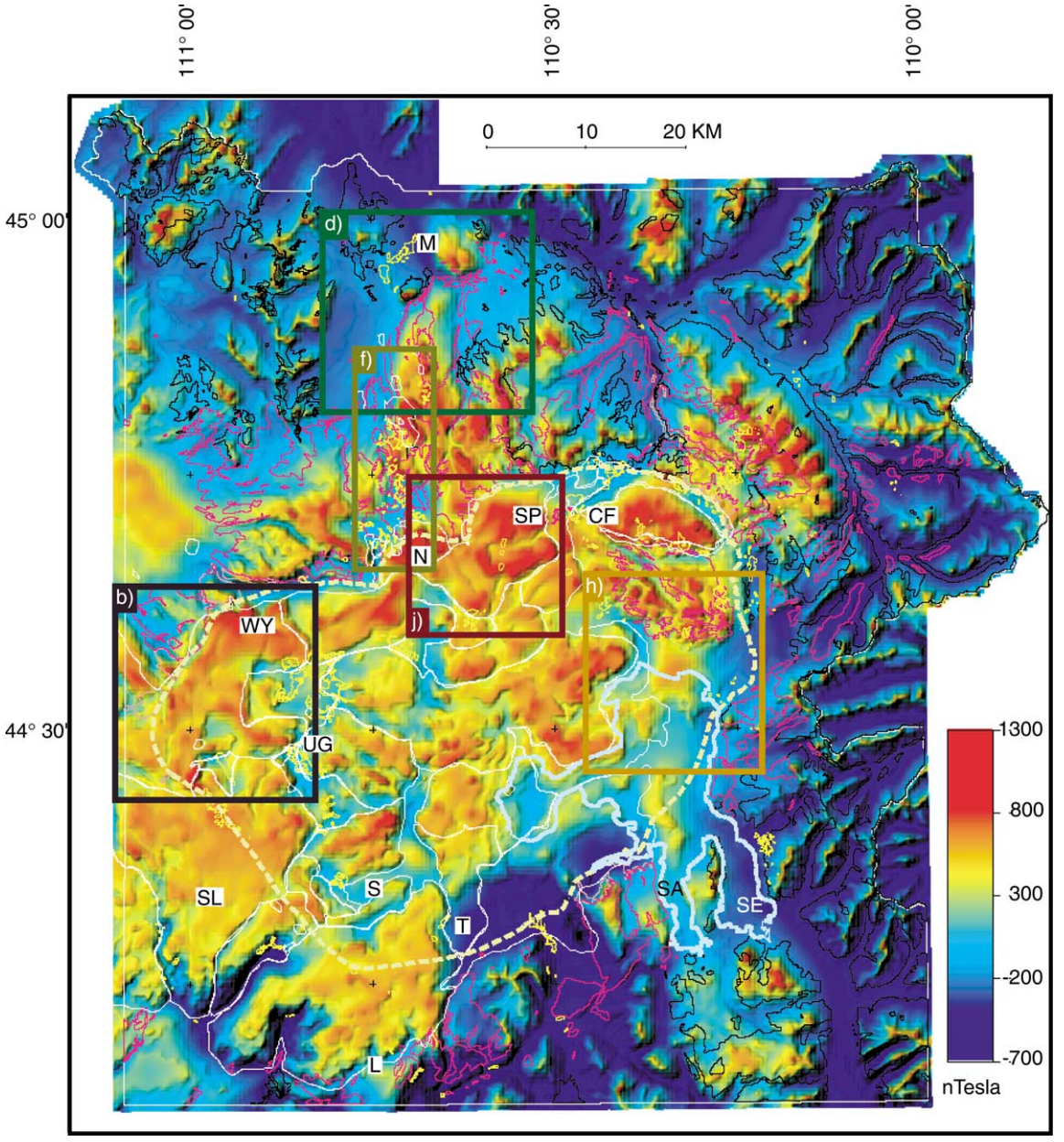

Fig. 5. Color shaded-relief image of the magnetic anomaly due to terrain uniformly magnetized in the present Earth's field direction of inclination = 70°, declination = 15° and intensity = 2.5 A/m and then reduced to the pole. Same legend as for Fig. 4.

the South Arm. West of the South Arm, the Quaternary Lava Creek Tuff is exposed. Based on similarities in magnetic expression to the Tertiary andesites, we suggest that the Lava Creek Tuff at this location is a thin veneer covering a much thicker sequence of Tertiary andesitic lavas. The shape of the low mimics the basement topography as defined by seismic reflection data (Otis et al., 1977), again suggesting that the Tertiary volcanic rocks continue beneath this part of the lake. Recent surveys with a submersible remotely operated vehicle in this area of the lake have collected mul-

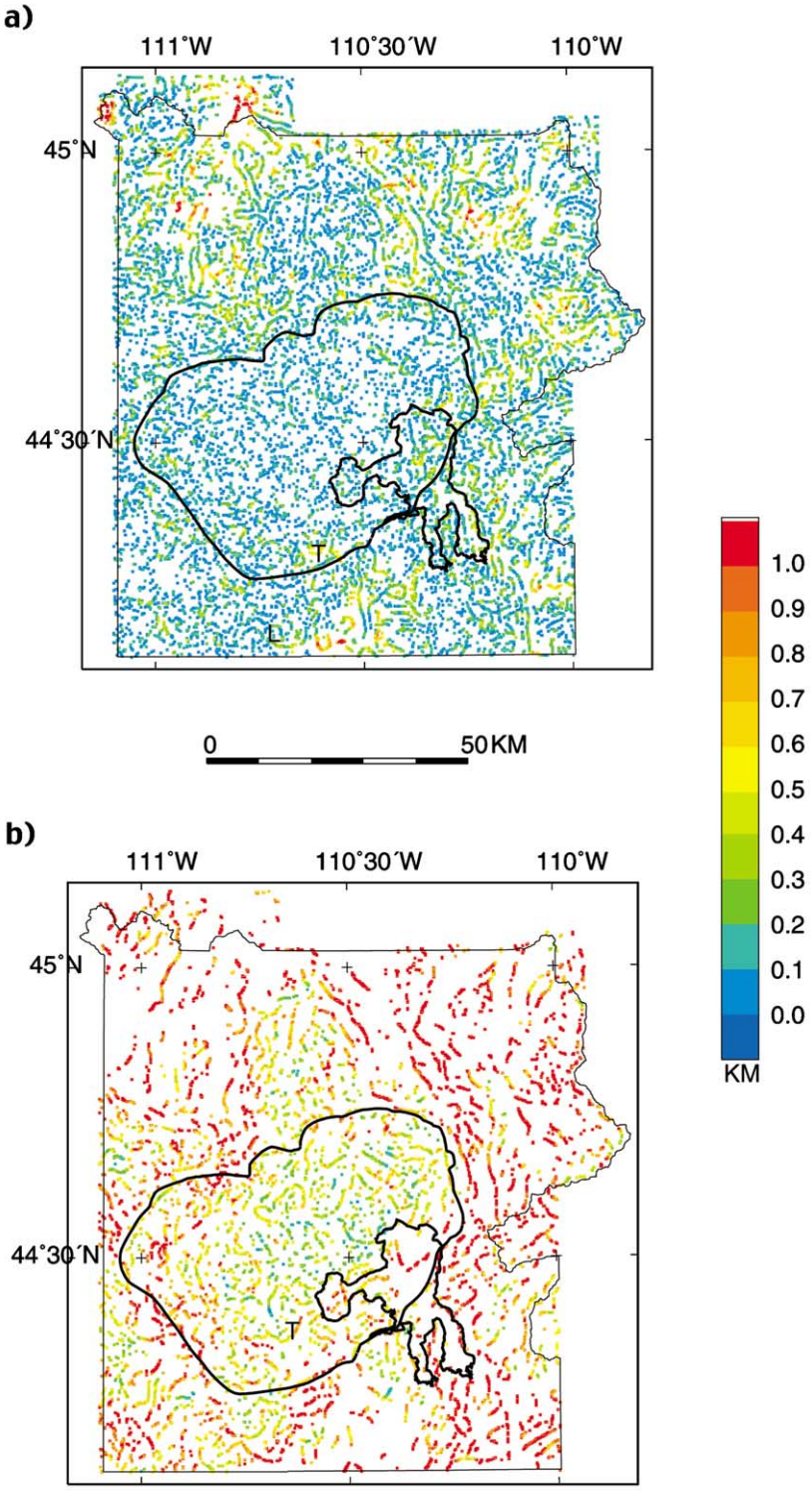

Fig. 6. (a) Estimates of depths of sources at the locations of the maximum horizontal gradients of the reduced-to-the-pole aeromagnetic data. (b) Estimates to depths of sources at the locations of the maximum horizontal gradients of the pseudo-gravity data.

tiple Tertiary volcanic rocks from the lake floor (Morgan et al., in press).

3.2. Stage 1: pre-Yellowstone caldera events

The regional tectonic stress field during the earliest stage (1.23 Ma) of the most recent caldera development at YNP is reflected in the major, active northwest- and north-trending faults associated with Basin and Range extension (Fig. 1). Comparison of the location of these faults with the location of linear magnetic gradients shows a general correlation where the faults cut magnetic rocks (Fig. 7). The faults are primarily visible north and south of the Yellowstone caldera (Fig. 1). However, one of these fault systems (Eagle Bay Fault) may extend from the south (Fig. 1; locality B, Fig. 7) north through Yellowstone Lake and may be associated with the older 2.1-Ma Huckleberry Ridge caldera margin (Fig. 2a). Focal mechanisms for earthquakes suggest normal faulting along this system (Smith et al., 1977).

Some of the pre-caldera lava flows whose remanent magnetizations are of reversed polarity (Table 1) do not produce magnetic lows on the map, indicating that they are thin. An example is the 0.929 ± 0.009-Ma Lewis Canyon flow (Obradovich, 1992; Table 1) in the southern-most area of the Park near 110°45'W longitude (locality L, Fig. 4). There, the positive anomaly expected from the uniformly magnetized terrain model (locality L, Fig. 4) corresponds to the observed magnetic data. In addition, the estimated depths to the sources in that area (locality L, Fig. 6a) are about 200–800 m below the surface. The Q values are also low (L.A. Morgan and S.S. Harlan, unpublished data). All of these observations suggest that the reversed part of the Lewis Canyon flow is too thin to produce a magnetic low. Conversely, in the western area of the map, the reversely magnetized member of the Mount Jackson Rhyolite, the 0.839 ± 0.007-Ma Harlequin Lake flow (Christiansen and Blank, 1972; Obradovich, 1992), produces magnetic lows (L.A. Morgan and S.S. Harlan, unpublished data) around the caldera boundary (Fig. 4, R, box a; Fig. 8a) and may extend southwest along the ring-fracture zone. The estimated depths to magnetic sources are less than 200 m (Fig. 6), indicating a surficial origin. The association of magnetic lows with the exposed flows suggests that the reversed part of the flow may be thicker and more extensive than the 0.640-Ma normally magnetized (Christiansen and Blank, 1972; Obradovich, 1992) Mount Haynes member exposed nearby.

During stage 1, pre-caldera basaltic eruptions occurred outside the Yellowstone caldera (Fig. 2a). In comparing the magnetic data (Fig. 4) with the uniformly magnetized terrain data (Fig. 5) for the pre-caldera Undine Falls Basalt, we observed linear, positive magnetic anomalies (Fig. 4, box c; Fig. 8c) unrelated to topography (Fig. 5, box d; Fig. 8d). The positive magnetic anomalies of the Undine Falls Basalt extend farther than its mapped extent indicating that this unit continues under the adjacent sedimentary rocks (UB, Fig. 8c).

3.3. Stage 2: cataclysmic eruption of the Lava Creek Tuff and formation of the Yellowstone caldera

The Lava Creek Tuff is normally magnetized with remanent intensities ranging from 0.7 to 10.0 A/m (Table 1) and a wide range of bulk magnetic susceptibilities typical of densely welded ignimbrites exposed in a young, thermally active volcanic terrain (Morgan and Christiansen, 1998; Reynolds, 1977). Its alteration states range from fresh, unaltered glass with typical susceptibilities of 6×10^{-3} SI to extensive kaolinitic alteration with susceptibilities near 2×10^{-6} SI (Morgan and Christiansen, 1998). The low magnetic susceptibility values for the hydrothermally altered rock are due to destruction of titanomagnetite during the alteration process. This wide range of bulk susceptibility values precludes clear identification of the Lava Creek Tuff as an individual geologic unit on the high-resolution aeromagnetic map. The total magnetization values (Table 1) are high enough to produce positive magnetic anomalies over thick (>50–100 m) sections of the ignimbrite. Thus, positive anomalies from the Lava Creek Tuff are expected where it is exposed in elevated terrain; such anomalies are observed northeast of the caldera and along the Mam-

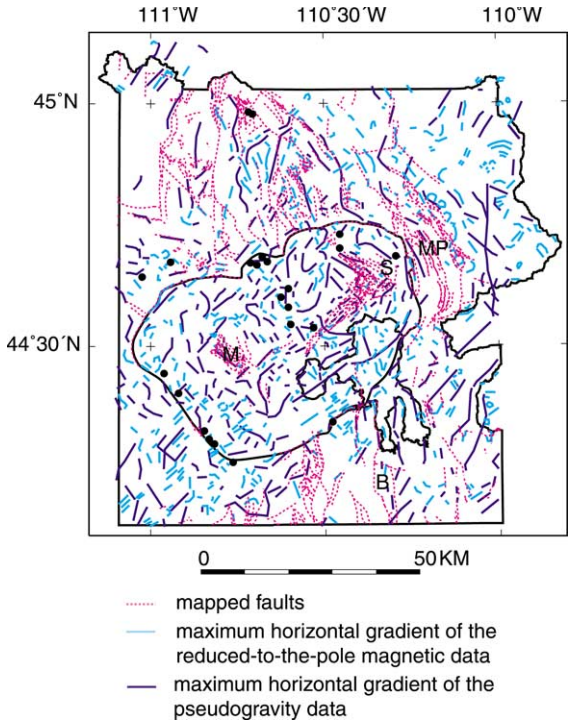

Fig. 7. Map showing the maximum horizontal gradient of the pseudo-gravity (purple lines) and reduced-to-the-pole (blue lines) transformations of the magnetic field. (a) Dashed magenta lines represent mapped faults (from U.S. Geological Survey, 1972). B = Eagle Bay Fault; M = Mallard Lake dome; S = Sour Creek dome and MP = Mirror Plateau. Solid dots represent vents for the post-caldera lavas (from Christiansen, 1984).

moth–Norris corridor (area south of Mammoth (M) to the caldera boundary, Figs. 4 and 5).

The mostly buried boundary of the Yellowstone caldera is defined along its northwestern, northeastern, and eastern boundaries on the aeromagnetic map (Fig. 4) by a series of discontinuous, negative magnetic anomalies reflecting low topography (Fig. 5) and faults (Fig. 1). An additional series of discontinuous negative anomalies within the topographic margin may reflect the now-buried caldera ring-fracture zone (Fig. 2b) as originally proposed by Christiansen (1984). On the gradient map (Fig. 7), the topographic boundary of the Yellowstone caldera and its inner ring-fracture zone appear as a disconnected series of lines.

3.4. Stage 3: post-Yellowstone caldera events

Post-caldera rhyolitic activity was initially concentrated near one of the caldera's two resurgent domes with eruption of the Canyon flow unit of the Upper Basin member of the Plateau rhyolite north of the Sour Creek dome (Figs. 1 and 2c). Similar to many of the other post-caldera rhyolitic lava flows, the Canyon flow does not have a magnetic signature that matches that expected from the terrain (CF, Figs. 4 and 5). In this example, the calculated anomaly due to terrain has a higher amplitude (Fig. 5) than the observed (Fig. 4), indicating that the actual intensity of magnetization of the Canyon flow is lower than that estimated. This discrepancy could be caused by the physical state of the lava flow. Some areas, such as internal fracture zones associated with thermal shrinkage of the initial flow or along edges of flows, are highly altered compared to other parts of the flow, such as glassy flow tops which remain unaltered. Field observations suggest many of the rhyolitic lava flows interacted with water and are hydrothermally altered to various extents. The magnetic data may map the buried continuation of a post-caldera rhyolite flow under Shoshone Lake (Fig. 1). The continuation of the positive magnetic anomaly associated with the southern part of the Spring Creek Flow (S, Figs. 4 and 5) over the west side of Shoshone Lake suggests that the flow underlies this part of the lake.

Correlation of magnetic highs with terrain anomalies of the West Yellowstone (WY) and Summit Lake (SL) rhyolite lava flows along the western edge of the caldera (Figs. 4 and 5) suggests that they are the primary sources of the anomalies, corresponding well with the estimated actual intensity of magnetization. These units are not as extensively altered as many. In contrast, Eaton et al. (1975) interpreted these magnetic highs as buried Tertiary rocks based on the previous, low-resolution data. The regional magnetic low over the northern Summit Lake flow (north of SL, Fig. 4) may represent an area where the flow is thin (less than 50 m) and highly altered, or possibly underlain by less magnetic, altered, or older reversely magnetized flows.

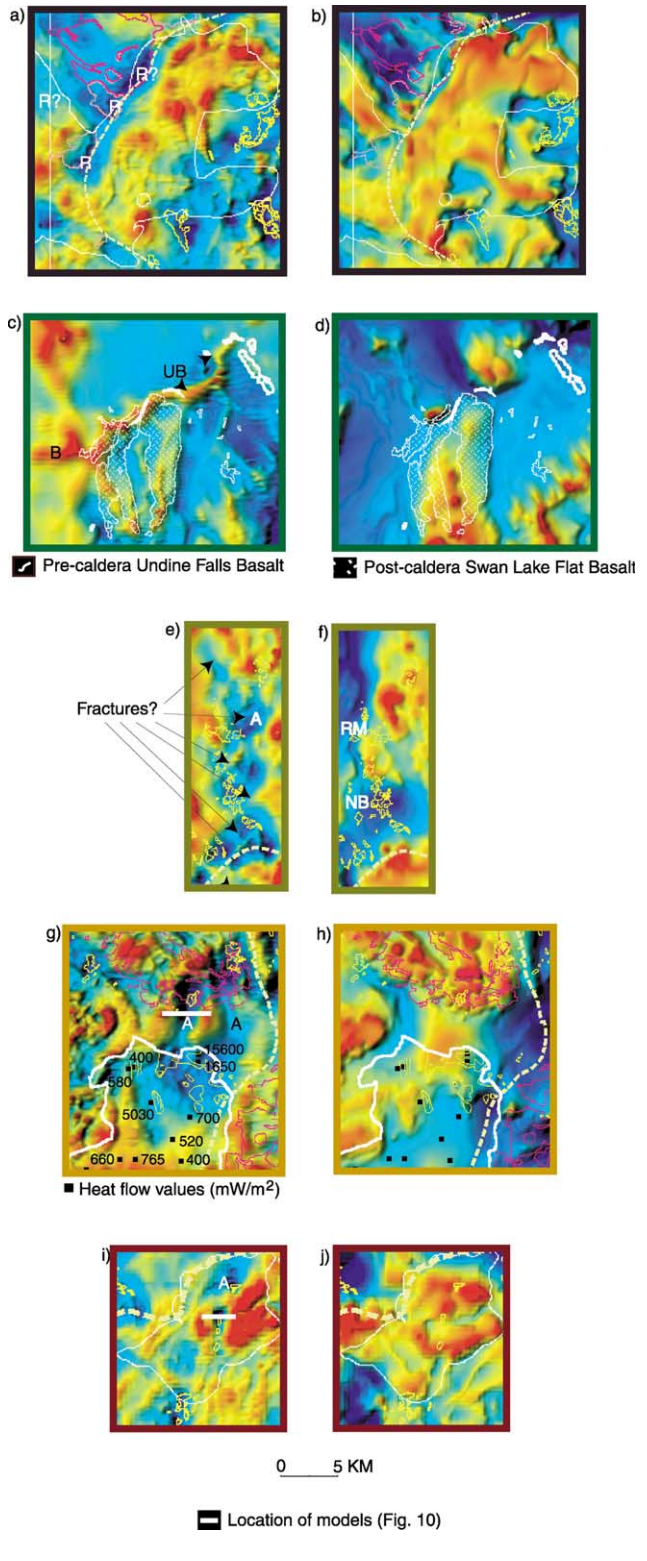
a)
b)
R?
R?
R
R
c)
d)
UB
B
Pre-caldera Undine Falls Basalt
Post-caldera Swan Lake Flat Basalt
e)
f)
Fractures?
A
RM
NB
g)
h)
A
A
15600
400
1650
580
5030
700
520
660
765
400
Heat flow values (mW/m2)
i)
j)
A
0 5 KM
Location of models (Fig. 10)

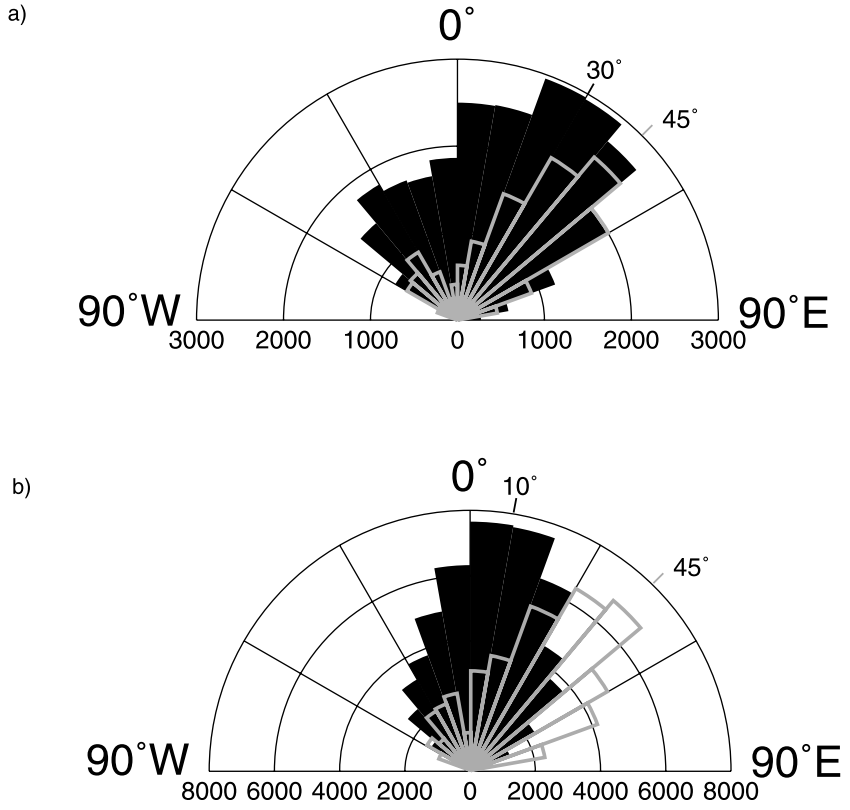

Fig. 9. Rose diagrams showing directions of trends of the maximum horizontal gradient of (a) the reduced-to-the pole magnetic (Fig. 4) and (b) pseudo-gravity data. Black colors indicate trends outside the caldera; gray lines show trends within the caldera. SE and SW trends are mapped into the NW and NE quadrants, respectively.

Basaltic activity continued intermittently throughout stage 3 with eruptions restricted to areas outside of the caldera. The aeromagnetic data are useful in delineating the areal extent of some of the post-caldera basalt flows; in other cases the aeromagnetic data may reveal more about the feeder dikes of the basalt flows. For example, the mapped extent of the Swan Lake Basalt is greater than the observed linear magnetic anomalies with which it is associated on the high-resolution magnetic maps (Fig. 8c,d). The north-trending positive magnetic anomalies may reflect fissures or feeder dikes within the basalt flows or areas where the flow is relatively thick or ponded (Fig. 8c). The north trend of the magnetic anomalies parallels the orientation of faults and the Norris–Mammoth corridor (Fig. 1) (Pierce et al., 1991).

Fig. 8. See Fig. 4 for polygon boundaries. (a, c, e, g and i) Close-ups of the observed reduced-to-the-pole magnetic data (locations shown in Fig. 4). (b, d, f, h and j) Close-ups of the magnetic anomaly due to uniformly magnetized terrain (locations shown in Fig. 5). (a, b) The area of the West Yellowstone post-caldera rhyolite lava flow. R denotes reversely magnetized Mount Jackson Rhyolite. R? marks the location of a suspected continuation of the flow. (c, d) UB and B indicate areas where the magnetic data indicate the unmapped extension of the flows of Undine Falls and Swan Lake Flat basalts, respectively (map polygons from Fig. 1). (e, f) RM = Roaring Mountain; NB = Norris Geyser Basin. NE- and NW-trending gradients (shading) indicate inferred unmapped fractures. (g, h) Heat flow values from Morgan et al., 1977; locations of alteration and fissures (lines in yellow) in Yellowstone Lake digitized from Kaplinski (1991). (i, j) The area of the Solfatara Plateau post-caldera rhyolite flow. A = inferred areas of unmapped alteration.

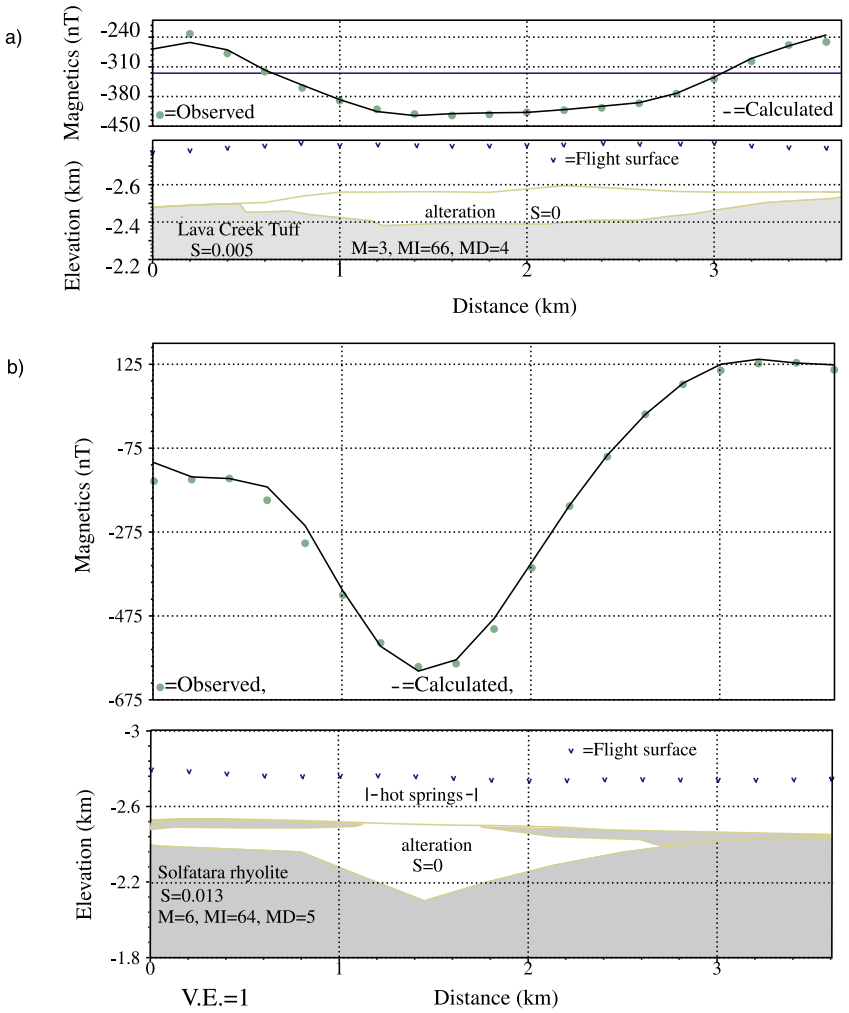

Fig. 10. Models of sources for the observed magnetic lows. The present Earth's field direction of inclination 70°, declination of 15° and intensity of 56 100 nT. To eliminate end effects, the models were continued with the layers shown at the ends of the section out to ±1000 km. Perpendicular to the profile, the blocks were extended ±3–5 km. S = susceptibility in SI units, M = intensity in A/m, MI = inclination in degrees, and MD = declination in degrees of remanent magnetization. (a) Profile across the Lava Creek Tuff (location of profile shown in Fig. 8e). (b) Profile across the Solfatara Plateau rhyolite flow (location of profile shown in Fig. 8i).

The present-day regional stress pattern is reflected in the gradients of the reduced-to-the-pole magnetic and pseudo-gravity data (Figs. 7 and 9). The predominant strikes of the reduced-to-the pole magnetic gradients are northeast within the Yellowstone caldera (Fig. 7, blue lines; Fig. 9a, gray lines) and to a lesser degree northwest and north outside the caldera (Fig. 7, blue lines; Fig. 9a, black lines). The strong northeast trend to the magnetic and pseudo-gravity gradients, particularly visible in the intra-caldera gradients (Figs. 7 and 9, gray lines), is reflected at the surface in the Elephant Back fault system (pink lines between S and M, Fig. 7) and in the elongation of the caldera. These trends parallel the orientation of the Snake River Plain to the southwest and were also observed in the low-resolution magnetic data over YNP (Fig. 3) and its surrounding region. In contrast, outside the caldera, the predominant trends of the gradients of the pseudo-gravity

are closer to north–south (Fig. 7, purple lines, and Fig. 9b, black lines). These trends mimic the trends of Basin and Range faults in the region (Fig. 7, pink lines). The pseudo-gravity gradients (Fig. 7, purple lines) generally reflect deeper (Fig. 6b) and more regional sources than the reduced-to-the-pole gradients (Fig. 6a).

Specific faults can be identified on the gradient map (Fig. 7). East-trending gradients in the west–central part of YNP (Fig. 7) correspond to faults that are mapped as part of the active Hebgen Lake seismic zone (Smith et al., 1977). This is one of the few areas in YNP with gradients of that trend and is a continuation of the Neotectonic fault belts along the western arm of the crescent of high terrain (Pierce and Morgan, 1992). Clear correlation between mapped faults and gradients also can be observed over the Mirror Plateau, the Sour Creek and Mallard Lake resurgent domes (MP, S, and M, respectively, Fig. 7), and along the northeast-trending, 0.153 ± 0.002-Ma (Obradovich, 1992) Elephant Back fault system (between S and M, Fig. 7). The pattern of northeast- and northwest-trending anomalies over the Norris–Mammoth area (Figs. 7 and 8e) is 45° from the main north-trending structures along this young post-caldera corridor. East of 110°45'W (Figs. 4 and 7), north-trending magnetic gradients generally coincide with some of mapped faults north of the caldera along a broad zone parallel to and including the Norris–Mammoth corridor. Northwest and south of the caldera, most of the mapped faults cannot be observed in the magnetic gradients (Fig. 7) because they cut non-magnetic sedimentary rocks.

3.5. Stage 4: later hydrothermal activity

In the final stages of a single caldera cycle, hydrothermal activity is prevalent throughout the entire system as evidenced today on the Yellowstone Plateau (Figs. 2d and 4, yellow lines). Locating active and extinct systems enables us to learn about the manner in which they have migrated over time. Hydrothermal alteration typically destroys the magnetic signature of volcanic rocks either by removing iron completely or by converting titanomagnetite to hematite, which has very low magnetic susceptibility. Therefore, if a volcanic rock is normally magnetized but altered, it could produce magnetic lows rather than highs. All areas of mapped acid hydrothermal alteration in YNP are associated with pronounced magnetic lows (Fig. 4).

In the Norris Geyser Basin and Roaring Mountain areas (NB and RM, Fig. 8e,f), northeast-trending oval magnetic lows are cut by northeast- and northwest-trending linear magnetic highs (Fig. 8e) unrelated to topography (Fig. 8f). Parts of these lows are associated with mapped areas of hydrothermal alteration, suggesting that continuation of the lows represents areas of unrecognized alteration. Low electrical resistivities have been interpreted to suggest that highly altered rocks underlie the surface in this region (Stanley et al., 1991).

The observed positive magnetic anomaly over the Lava Creek Tuff in the Sour Creek resurgent dome (Fig. 1) is similar to that expected from the elevated topography except in the southeast corner where hydrothermal alteration has occurred (Fig. 4, box g; Fig. 5, box h; Fig. 8g,h). This area of the Sour Creek dome is also the site of a post-glacial (less than 12 000 yr) hydrothermal explosion crater (Morgan et al., 1998). Within the Sour Creek resurgent dome, the magnetic low extends beyond the mapped alteration and is concentrated along the rectilinear fault system associated with the resurgent dome. Magnetic lows (A, Fig. 8g) extend over the dome and Quaternary sediments, south to the northeastern part of Yellowstone Lake and are unrelated to topography (Fig. 8h. This area has some of the highest heat flow in the lake (1650–15 600 mW/m^3, Fig. 8g) and contains numerous post-glacial hydrothermal explosion craters ranging in diameter from less than 0.5 km to more than 2 km. This area also is along the eastern margin of the Yellowstone caldera where significant fault displacement may have occurred resulting in Tertiary andesitic volcanic rocks exposed to the east abutting post-caldera rhyolites to the west (Fig. 1). Magnetic data collected from a sensor towed over the northern part of Yellowstone Lake detected high-frequency magnetic lows over the edges of small basins (Morgan et al., 1999; Wold et al., 1977), inter-

preted to be hydrothermal explosion craters. These lows are most likely caused by hydrothermal alteration of the host strata along caldera-related faults and through sublacustrine hydrothermal vents (Morgan et al., 1998; Shanks et al., 1997).

High heat flow (5030 mW/m^2, Morgan et al., 1977; Fig. 8g) also has been measured nearby in the northwestern section of Yellowstone Lake where faults have been located from seismic reflection data (Otis et al., 1977; Kaplinski, 1991) and numerous hydrothermal vent sites have been located using high-resolution multi-beam sonar imaging (Morgan et al., 1999). This area of high heat flow is also associated with a magnetic low although a magnetic high would be predicted from the bathymetry (Fig. 8g,h), suggesting that the observed magnetic lows in this part of Yellowstone Lake are probably caused by altered volcanic rocks associated with active hot springs. In contrast to the magnetic low related to bathymetry over the Southeast Arm of Yellowstone Lake (SE, Figs. 4 and 5), the eastern part of the South Arm (SA, Figs. 4 and 5) corresponds to a linear, high-amplitude magnetic low, unexplained either by topography (Fig. 5) or depth to magnetic basement determined by seismic data (Otis et al., 1977). The depth estimates indicate shallow sources (Fig. 6). Many hot springs occur along the mapped fault to the west of the South Arm, suggesting that hydrothermal alteration along a fault might be the source of the low. This area coincides with the north-trending Basin and Range fault system coincident with the more active parts of the Neotectonic fault belts (Pierce and Morgan, 1992). A good example of hydrothermal alteration reducing the intensity of magnetization in the post-caldera rhyolites can be observed in the Solfatara Plateau where magnetic lows not correlated with terrain are observed (SP, Figs. 4 and 5; Fig. 8i,j). A marked north-trending magnetic low associated with three areas of mapped alteration bisects the high associated with the unaltered parts of the flow. In addition, the magnetic lows extend laterally beyond the mapped areas of alteration, for distances as great as 2 km (near A, Fig. 8i), and occur where alteration has not been observed.

Modeling of the magnetic data can be used to estimate the volume of altered rock, thus providing evidence for the minimum extent of the hydrothermal system. The qualitative interpretation presented above gives information on the lateral extent of the hydrothermally altered areas that cause the observed magnetic anomalies. To estimate thickness of the altered areas, computer modeling is necessary. In order to determine the structures and magnetizations that produce the observed magnetic anomalies, we used a commercial 2.5-dimensional forward and inverse magnetic modeling software package. The program uses profiles of magnetic observations and a starting model consisting of body corners and magnetization contrasts. The program then adjusts the starting model so that its magnetic attraction fits the profiles of observed data. Allowing only a few parameters to vary in each modeling attempt and constraining those parameters to a specified range control the evolution of the final model.

In modeling, there is a trade-off between volume and magnetization of a given material. Given the maximum expected magnetization for the Lava Creek Tuff (Reynolds, 1977) and the post-caldera rhyolites, and the minimum magnetization expected for completely altered material (0 A/m), minimum thicknesses can be estimated for the altered areas. We constructed magnetic models across the Lava Creek Tuff at the Sour Creek dome (Fig. 8g) and the Solfatara Plateau rhyolite flow (Fig. 8i). In both models, we applied the induced magnetization direction of the present day field with inclination 70°, declination 15°, and intensity of 56 100 nT.

The Lava Creek Tuff has an average remanent magnetization with an inclination of 66°, declination of 4°, and intensity of 6 A/m (Reynolds, 1977; Table 1). A maximum value for the susceptibility of the ignimbrite is about 6×10^{-3} SI (Oliver and Christiansen, 1998; L.A. Morgan and S.S. Harlan, unpublished data). Using these values, the minimum model thickness of the altered part of the Lava Creek Tuff near the Sour Creek dome is about 200 m (Fig. 10a).

The remanent magnetization of the Solfatara Plateau rhyolite has an inclination of 64°, declination of 5°, and intensity near 5 A/m and a sus-

ceptibility of 6.5×10^{-4} SI (Table 1). A maximum susceptibility value for the Quaternary rhyolites is about 6×10^{-3} SI (Oliver and Christiansen, 1998). Applying these values to the model yields a minimum thickness for the altered area in the Solfatara Plateau rhyolite flow of about 400 m (Fig. 10b). Lower values of magnetization for the rhyolites would yield greater thicknesses for the altered zone. In both cases, the interpreted altered material extends laterally beyond the areas of mapped alteration and is about 2–3 km wide. The models show that a thin veneer of unaltered surficial volcanic rock overlies much of the altered material. The variations in thicknesses between the models may reflect physical differences in the character of the volcanic rocks, a more focused hydrothermal system, a more developed and larger fracture system, or different chemistry of the hydrothermal fluids in the Solfatara Plateau flow as compared to the Lava Creek Tuff in the Sour Creek dome.

Close inspection of the maps shows that most of the magnetic lows associated with known hydrothermal areas are ovals about 1.5–6 km in diameter bounded by steep gradients (see lows associated with hydrothermal alteration, Fig. 8e,g,i). Depth estimates from the magnetic data and correlation with mapped hydrothermal alteration show most of these areas to be at or near the surface (Fig. 6). Many of the magnetic lows are broader than the areas associated with active hot springs and associated mapped alteration (Fig. 4). The extensions of these lows may indicate areas where lateral flow of geothermal fluids is currently altering the subsurface rocks or may reflect the locations of fossil hot springs (e.g. Fig. 8e,i). This may also be true for those magnetic lows completely unassociated with mapped alteration (e.g. A, Fig. 8g; the northwest-trending region of circular lows near 110°45'W longitude between 44°20'N and 44°32'N (north of S, Fig. 4)). The magnetic lows related to hydrothermal alteration are spaced at distances less than a few kilometers throughout the caldera and Norris–Mammoth corridor areas. This pattern may represent convective cells of hydrothermal systems with spacing between the vertical axes of cells of less than a few kilometers. If these are truly convection cells, they would suggest a very different model for fluid flow (K.L. Pierce and W.C. Shanks, written communication, 1999) than one which predicts long distance flow of water from mountainous source areas to the major geyser basins (Rye and Truesdell, 1993).

The steep gradients that bound the magnetic lows over the altered zones may reflect fracture systems that have localized hot springs. These inferred fractures as well as other regional magnetic lineations are oriented northeast, northwest, and north (Figs. 7 and 9), in many cases paralleling regional tectonic trends. The northwest-trending region of magnetic lows mentioned above (north of S, Fig. 4) is associated with steep, northwest-trending magnetic gradients (Fig. 7) suggesting that fractures localized hydrothermal systems that altered the volcanic rocks. Hydrothermal activity in Yellowstone Lake is often concentrated along the edges and selected interior portions of rhyolitic lava flows recognized in high-resolution bathymetric surveys as well as several fissure systems of various orientations (Morgan et al., in press). Hydrothermal vents (Shanks et al., 1997) or fissures oriented approximately northeast to northwest are located in the intensely active northeast portion of the lake where heat flow values exceed 1600 mW/m^2 (Fig. 8g) (Morgan et al., 1977). This alignment of hydrothermal activity may, in part, be controlled by faults that are part of a regionally extensive normal fault system (e.g. Eagle Bay Fault, B, Fig. 7) related to regional extension (Morgan et al., in press). The 1-km-wide magnetic lows in the northeast part of the lake (Fig. 8g) trend northeast to northwest and are bounded by steep gradients. This pattern suggests that fractures have localized small extensional basins and hydrothermal activity. Morgan et al. (1977) speculated that many of the high heat flow values in Yellowstone Lake occurred over hot springs localized by fractures. The correspondence of the linear magnetic gradients with high heat flow values supports this interpretation. Outside the lake, extension may produce the basins in which hydrothermal activity is often concentrated.

Fractures provide paths for migration of hydrothermal activity. An example can be observed in the Norris Geyser Basin–Roaring Mountain area where magnetic lows associated with alteration

caused by active hydrothermal hot springs are linked by inferred fractures to lows over areas lacking current hydrothermal activity to the northeast (Fig. 8e). Northeast-oriented joints, coincident with the prevailing trend of local streams, have been observed further to the northeast along this trend (K.L. Pierce, written communication, 1999) suggesting a regional control on the fracture pattern. Further evidence of the fracture control on hydrothermal activity is provided by the good correlation of seismicity with onset of hydrothermal activity (Pitt and Hutchinson, 1982). This suggests that seismic slip may occur on the boundaries of small upper crustal blocks, which may reflect a combination of deformation caused by local magmatic and hydrothermal fluid transport and by the regional stress field (Smith and Braile, 1994).

On a more regional scale, the active faults in the region that trend generally north–south relate to active Basin and Range extension as well as uplift related to the passage of the Yellowstone hot spot (Pierce and Morgan, 1992). Stress field directions in the region obtained from various data sets are also compatible with east–west extension (Dzurisin et al., 1990; Smith and Braile, 1994). The primary strike directions of the pseudo-gravity gradients outside the caldera follow the regional north–south fault trends. Because the pseudo-gravity data sense regional and/or deep features, this suggests that extension in the Basin and Range stress field dominates the structural development in YNP from small-scale hydrothermal systems to regional faults.

Active northwest-trending faults north of the Yellowstone caldera probably represent reactivated Precambrian weaknesses in the basement. The northeast trends, particularly pronounced within the caldera (Fig. 7), partially reflect northeast-trending faults present in the post-caldera Elephant Mountain rhyolite lavas and northeast elongation of the Yellowstone caldera. The northeast trends may also be influenced by regional northeast-trending tectonic zones, which are subparallel to the northeast trend of the eastern Snake River Plain. The Great Falls tectonic zone (O'Neill and Lopez, 1985) is located 200 km north while the Madison mylonite zone (Erslev et al., 1982; Erslev and Sutter, 1990) is 30 km north of the Yellowstone–Snake River Plain volcanic province. These northeasterly directions are parallel to the structural grain of Precambrian basement rocks to the north.

Despite caldera collapse and eruption of large volumes of magma, as well as deformation associated with magma injection (Pelton and Smith, 1982; Dzurisin et al., 1990), magnetic trends and structures do not seem to follow a pattern related to the underlying batholith. Instead, the Precambrian structural grain to the north and south of the Yellowstone caldera appears in magnetic gradients as well as fault patterns and localization of various hydrothermal systems. This suggests that reactivation of older crustal weakness may play a role in the tectonic evolution of the region, including the collapse of the caldera. The Lava Creek Tuff and subsequent magmatism could have erupted through faults and extensional basins localized by pre-existing zones of weakness.

4. Discussion

High-resolution aeromagnetic data provide a sharper view of the geology of YNP than previously available. The distinct magnetic signatures of several mapped flows demonstrate the utility of the magnetic data for delineating flows and flow margins. Extensions of several lava flows beneath younger cover have been identified. Rock property and stratigraphic thickness measurements can help constrain the extents of other lava flows.

The effects of the extensive hydrothermal system can be observed in the magnetic data in the form of magnetic lows due to altered volcanic rocks. The extents of these lows constrain the locations of modern and past hydrothermal activity and give information on the intensity of this activity in individual areas. Understanding the distribution of heat and hydrothermal vents beneath lakes in YNP will increase knowledge of the interplay between the geology and the ecosystem.

Linear gradients observed in the magnetic data follow regional tectonic trends, not local ones related to magmatic activity. The correspondence of some gradients to mapped faults and locations of

hot springs strongly suggests that the linear magnetic gradients represent faults and fractures. Future field studies of the aeromagnetic lineaments defined in this paper combined with information from other data sets may provide a clear picture of the faults and fractures that localize hydrothermal systems as well as various aspects related to development of the Yellowstone caldera. In addition, the delineation of new faults with the aeromagnetic data may help to associate seismicity with faults and thereby improve seismic hazard assessments.

Acknowledgements

We thank Steve Harlan, Jeff Phillips, Ken Pierce, Rick Saltus, Pat Shanks, and an anonymous reviewer for their careful reviews. We also thank and acknowledge Greg Lee, Suzanne Miller, and Vicki Rystrom for their assistance in the preparation of several of the figures. This work was supported by the U.S. Geological Survey Mineral Resource Program.

References

Anders, M.H., Geissman, J.W., Piety, L.A., Sullivan, J.T., 1989. Parabolic distribution of circum-eastern Snake River Plain seismicity and latest Quaternary faulting: Migratory pattern and association with the Yellowstone hot spot. J. Geophys. Res. 94, 1589–1621.

Baranov, V., Naudy, H., 1964. Numerical calculation of the formula of reduction to the magnetic pole. Geophysics 29, 67–79.

Bath, G.D., 1968. Aeromagnetic anomalies related to remnant magnetism in volcanic rock, Nevada Test Site. Geol. Soc. Am. Mem. 110, 135–146.

Bhattacharyya, B.K., Leu, L.-K., 1975. Analysis of magnetic anomalies over Yellowstone National Park: mapping of Curie point isothermal surface for geothermal reconnaissance. J. Geophys. Res. 80, 4461–4465.

Blackwell, D.D., 1989. Regional implications of heat flow of the Snake River Plain, northwestern United States. Tectonophysics 164, 323–343.

Blakely, R.J., 1995, [Monograph] Potential theory in gravity and magnetic applications. Cambridge University Press, Cambridge, 441 pp.

Blakely, R.J., Simpson, R.W., 1986. Approximating edges of source bodies from magnetic or gravity anomalies. Geophysics 51, 1494–1498.

Christiansen, R.L., 1984. Yellowstone magmatic evolution: Its bearing on understanding large-volume explosive volcanism, Explosive volcanism: inception, evolution and hazards. Studies in Geophysics, National Academy Press, Washington, DC, pp. 84–95.

Christiansen, R.L., in press. The Quaternary and Pliocene Yellowstone volcanic field of Wyoming, Idaho, and Montana. U.S. Geological Survey Professional Paper, 729-G.

Christiansen, R.L., Blank, H.R., 1972. Volcanic stratigraphy of the Quaternary rhyolite plateau in Yellowstone National Park. USGS Professional Paper, 729B, p. 18.

Christiansen, R.L., McKee, E.H., 1978. Late Cenozoic volcanic and tectonic evolution of the Great Basin and Columbia intermountain regions. In: Smith, R.B., Eaton, G.P. (Eds.), Cenozoic Tectonics and Regional Geophysics of the Western Cordillera. Geological Society of America Memoir 152, pp. 283–311.

Cordell, L., Grauch, V.J.S., 1982. Reconciliation of the discrete and integral Fourier transforms. Geophysics 47, 237–243.

Cordell, L., Grauch, V.J.S., 1985, Mapping basement magnetization zones from aeromagnetic data in the San Juan Basin, New Mexico. In: Hinze, W.J. (Ed.), The Utility of Regional Gravity and Magnetic Anomaly Maps. Society of Exploration Geophysics, Tulsa, OK, pp. 181–197.

Denham, D., 1997. Airborne geophysics in Australia: The Government Contribution. AGSO J. Aust. Geol. Geophys. 17, 3–9.

Dzurisin, D., Savage, J.C., Fournier, R.O., 1990. Recent crustal subsidence at Yellowstone Caldera, Wyoming. Bull. Volcanol. 52, 247–270.

Eaton, G.P., Christiansen, R.L., Iyer, H.M., Pitt, A.M., Mabey, D.R., Blank, H.R., Jr., Zietz, I., Gettings, M.E., 1975. Magma beneath Yellowstone National Park. Science 188, 787–796.

Erslev, E.A., Reid, S.G., Foote, D.J., 1982. The Madison mylonite zone; a major shear zone in the Archean basement of southwestern Montana, Wyoming Geological Association 33rd annual field conference. Geology of the Yellowstone National Park area, Mammoth Hot Springs, WY, 33, pp. 213–221.

Erslev, E.A., Sutter, J.F., 1990. Evidence for Proterozoic mylonitization in the northwestern Wyoming Province; with Suppl. Data 90-24. Geol. Soc. Am. Bull. 102, 1681–1694.

Fournier, R.O., 1989. Geochemistry and dynamics of the Yellowstone National Park hydrothermal system. Annu. Rev. Earth Planet. Sci. 17, 13–53.

Fournier, R.O., White, D.E., Truesdell, A.H., 1976. Convective heat flow in Yellowstone National Park. Proceedings of the Second U.N. Symposium Development and Use of Geothermal Resources, San Francisco 1975, Washington, DC, U.S. Government Printing Office, pp. 731–739.

Gansecki, C.A., Mahood, G.A., McWilliams, M., 1998. New ages for the climactic eruptions at Yellowstone; single-crystal $^{40}Ar/^{39}Ar$ dating identifies contamination. Geology 26, 343–346.

Gansecki, C.A., Mahood, G.A., McWilliams, M.O., 1996.

$^{40}Ar/^{39}Ar$ geochronology of rhyolites erupted following collapse of the Yellowstone Caldera, Yellowstone Plateau volcanic field; implications for crustal contamination. Earth Planet. Sci. Lett. 142, 91–108.

Grauch, V.J.S., Hudson, M.R., 1987. Summary of natural remanent magnetization, magnetic susceptibility, and density measurements from the Lake City Caldera area, San Juan Mountains, Colorado. U.S. Geological Survey Open-File Report 87-182, 23 pp.

Grauch, V.J.S., Sawyer, D.A., Friedrich, C.J., Hudson, M.R., 1997. Geophysical Interpretations West of and Within the Northwestern Part of the Nevada Test Site. U.S. Geological Survey Open-File Report 97-476, p. 45.

Grauch, V.J.S., Millegan, S., 1998. Mapping intrabasinal faults from high-resolution aeromagnetic data. Leading Edge 17, 53–55.

Harlan, S.S., Snee, L.W., Geissman, J.W., 1996. $^{40}Ar/^{39}Ar$ geochronology and paleomagnetism of Independence volcanics, Absaroka Volcanic Supergroup, Beartooth Mtns, Montana. Can. J. Earth Sci. 33, 1648–1654.

Hildreth, W., Christiansen, R.L., O'Neil, J.R., 1984. Catastrophic isotopic modification of rhyolitic magma at times of caldera subsidence, Yellowstone Plateau volcanic field. J. Geophys. Res. 89, 8339–8369.

Kaplinski, M.A., 1991. Geomorphology and Geology of Yellowstone Lake, Yellowstone National Park, Wyoming (Masters thesis). Northern Arizona University, 82 pp.

Leeman, W.P., 1982. Rhyolites of the Snake River Plain–Yellowstone Plateau Province, Idaho and Wyoming: A Summary of Petrographic Models. In: Bonnichsen, B., Breckenridge, R.M. (Eds.), Cenozoic Geology of Idaho: Idaho Bureau of Mines and Geology Bulletin 26, pp. 203–212.

Leeman, W.P., 1989. Origin and development of the Snake River Plain; an overview. Geol. Soc. Am. Abstr. Programs 14, 180.

Lehman, J.A., Smith, R.B., Schilly, M.M., 1982. Upper crustal structure of the Yellowstone caldera from seismic delay time analyses and gravity correlations. J. Geophys. Res. 87, 2713–2730.

Locke, W.W., Meyer, G.A., Pings, J.C., 1992. Morphology of a postglacial fault scarp across the Yellowstone (Wyoming) caldera margin, United States, and its implications. Bull. Seismol. Soc. Am. 82, 511–516.

Morgan, L.A., Christiansen, R.L., 1998. Preliminary results from anisotropic magnetic susceptibility studies of the Lava Creek Tuff, Yellowstone National Park. In: Yellowstone Science, vol. 6. 125th Anniversary Symposium, Bozeman, MT, p. 42.

Morgan, L.A., Pierce, K.L., Christiansen, R.L., Lageson, D.R., 1998. 125 Years of Geologic Discovery in Yellowstone: A Progress Report. In: Yellowstone Science, vol. 6. 125th Anniversary Symposium, Bozeman, MT, p. 43.

Morgan, L.A., Shanks, W.C., Pierce, K.L., Rye, R.O., 1999. Hydrothermal explosion deposits in Yellowstone National Park: Links to hydrothermal processes: EOS, Transactions American Geophysical Union, Fall Annual Meeting, vol. 79, F964.

Morgan, L.A., Shanks, W.C., Lovalvo, D., Johnson, S.Y., Stephenson, W.J., Balistrieri, L., White, E.A., in press. The floor of Yellowstone Lake is anything but quiet: New discoveries from high-resolution sonar imaging, seismic reflection profiling, and submersible studies. Yellowstone Sci.

Morgan, P., Blackwell, D.D., Spafford, R.E., Smith, R.B., 1977. Heat flow measurements in Yellowstone Lake and the thermal structure of the Yellowstone caldera. J. Geophys. Res. 82, 3719–3732.

Muffler, L.J.P., White, D.E., Truesdell, A.H., 1971. Hydrothermal explosion craters in Yellowstone National Park. Geol. Soc. Am. Bull. 82, 723–740.

Nyblade, A.P., Shive, N., Furlong, K.P., 1987. Rapid secular variation in thick Eocene flows from the Absaroka Mountains of northwest Wyoming. Earth Planet. Sci. Lett. 81, 419–424.

Obradovich, J.D., 1992. Geochronology of the late Cenozoic volcanism of Yellowstone National Park and adjoining areas, Wyoming and Idaho. U.S. Geological Survey Open-File Report 92-048, 45 pp.

Oliver, H.W., Christiansen, R.L., 1998. Locations, descriptions, densities, and magnetic susceptibilities of rock samples collected for analysis of gravity and aeromagnetic anomalies in Yellowstone National Park, Wyoming, Idaho and Montana. U.S. Geological Survey Open-File Report 98-247.

O'Neill, J.M., Lopez, D.A., 1985. Character and regional significance of Great Falls tectonic zone, east–central Idaho and west–central Montana. AAPG Bull. 69, 437–447.

Otis, R.M., Smith, R.B., Wold, R.J., 1977. Geophysical Surveys of Yellowstone Lake, Wyoming. J. Geophys. Res. 82, 3705–3717.

Pelton, J.R., Smith, R.B., 1982. Contemporary vertical surface displacements in Yellowstone National Park. J. Geophys. Res. 87, 2745–2761.

Phillips, J.D., 1997. Potential-field geophysical software for the PC, version 2.2. U.S. Geological Survey Open-File Report 97-725.

Phillips, J.D., 1999. An interpretation of proprietary aeromagnetic data over the northern Arctic National Wildlife Refuge and adjacent areas, northeastern Alaska: in ANWR Assessment Team, The oil and gas potential of the 1002 area, Arctic National Wildlife Refuge, Alaska. U.S. Geological Survey Open-File Report 98-103.

Pierce, K.L., Adams, K.D., Sturchio, N.C., 1991. Geologic setting of the Corwin Springs Known Geothermal Resources Area–Mammoth Hot Springs area in and adjacent to Yellowstone National Park. In: Sorey, M.L. (Ed.), Effects of Potential Geothermal Development in the Corwin Springs Known Geothermal Resources Area, Montana, on the Thermal Features of Yellowstone National Park. U.S. Geological Survey Water-Resources Investigations 91-4052, pp. C1–C37.

Pierce, K.L., Morgan, L.A., 1992. The track of the Yellowstone hot spot: volcanism, faulting, and uplift. In: Link, K., Kuntz, M.A., Platt, L.B. (Eds.), Regional Geology of Eastern Idaho and Western Wyoming. Geological Society of America Memoir 179, pp. 1–53.

Pitt, A.M., Hutchinson, R.A., 1982. Hydrothermal changes related to earthquake activity at Mud Volcano, Yellowstone National Park, Wyoming. J. Geophys. Res. 87, 2762–2766.

Pruss, E.F., 1975. A paleomagnetic study of basalt flows from the Absaroka Mountains, Wyoming. Wyoming Geological Association Field Conference Guidebook, pp. 257–266.

Reynolds, R.L., 1977. Paleomagnetism of welded tuffs of the Yellowstone Group. J. Geophys. Res. 82, 3677–3693.

Rye, R.O., Truesdell, A.H., 1993. The question of recharge to the geysers and hot springs of Yellowstone National Park. U.S. Geological Survey Open-File Report 93-384, 40 pp.

Shanks, W.C., Alt, J.C. III, Meier, A.L., Klump, J.V., 1997. Geochemical studies of hydrothermal deposits related to sublacustrine hydrothermal vents in Yellowstone Lake. EOS, Transactions American Geophysical Union, Fall Annual Meeting, vol. 78, F808–F809.

Shive, N., Pruss, E.F., 1977. A paleomagnetic study of basalt flows from the Absaroka Mountains, Wyoming. J. Geophys. Res. 82, 3039–3048.

Smedes, H.W., Prostka, H.J., 1972. Stratigraphic framework of the Absaroka Volcanic Supergroup in the Yellowstone National Park region. U.S. Geological Survey Professional Paper 729-C, pp. C1–C33.

Smith, R.B., Braile, L.W., 1994. The Yellowstone hotspot. J. Volcanol. Geotherm. Res. 61, 121–187.

Smith, R.B., Sbar, N.L., 1974. Contemporary tectonics and seismicity of the western United States with emphasis on the Intermountain Seismic Belt. Geol. Soc. Am. Bull. 85, 1205–1218.

Smith, R.B., Shuey, R.T., Freidline, R.O., Otis, R.M., Alley, L.B., 1974. Yellowstone Hot Spot: New magnetic and seismic evidence. Geology 2, 451–455.

Smith, R.B., Shuey, R.T., Pelton, J.R., Bailey, J.P., 1977. Yellowstone Hot Spot: Contemporary tectonics and crustal properties from earthquake and aeromagnetic data. J. Geophys. Res. 82, 3665–3676.

Smith, R.L., Bailey, R.A., 1968. Resurgent cauldrons. In: Coats, R.R. (Ed.), Studies in Volcanology. Geological Society of America Memoir 116, pp. 5–27.

Stanley, W.D., Hoover, D.B., Sorey, M.L., Rodriguez, B.D., Heran, W.D., 1991. Electrical geophysical investigations in the Norris–Mammoth corridor, Yellowstone National Park, and the adjacent Corwin Springs Known Geothermal Resources Area. In: Sorey, M.L. (Ed.), Effects of Potential Geothermal Development in the Corwin Springs Known Geothermal Resources Area, Montana, on the Thermal Features of Yellowstone National Park. U.S. Geological Survey Water-Resources Investigations 91-4052, pp. D1–D18.

Sundell, K.A., Shive, P.N., Eaton, G.P., 1984. Measured sections, magnetic polarity and biostratigraphy of the Eocene Wiggins, Teepee Trail and Across Formations within the southeastern Absaroka Range, Wyoming. Earth Science Bulletin, Wyoming Geological Association, vol. 17, pp. 1–48.

U.S. Geological Survey, 1972. Geologic Map of Yellowstone National Park. Miscellaneous Geologic Investigations Map: I-711.

U.S. Geological Survey, 1973. Aeromagnetic Map of Yellowstone National Park and Vicinity, Wyoming–Montana–Idaho. U.S. Geological Survey Open-File Report 73-304.

U.S. Geological Survey, 2000, An Aeromagnetic Survey in Yellowstone National Park: A Web Site for Distribution of Data (on-line edition). U.S. Geological Survey Open-File-Report 00-163 (http://geology.cr.usgs.gov/pub/open-file-reports/ofr-00-0163/).

Wicks, C., Jr., Thatcher, W., Dzurisin, D., 1998. Migration of fluids beneath Yellowstone Caldera inferred from satellite radar interferometry. Science 282, 458–462.

Wold, R.J., Mayhew, M.A., Smith, R.B., 1977. Geophysical study of a hydrothermal explosion crater, Mary Bay, Yellowstone Lake, Wyoming. J. Geophys. Res. 82, 3733–3738.

Zoback, M.L., Thompson, G.A., 1978. Basin and Range rifting in northern Nevada: Clues from a mid-Miocene rift and its subsequent offsets. Geology 6, 111–116.